

Reference-Free 3D Reconstruction of Brain Dissection Photographs with Machine Learning

Lin Tian¹, Sean I. Young^{1,3}, Jonathan Williams Ramirez¹, Dina Zemlyanker¹, Lucas Jacob Deden Binder¹, Rogeny Herisse¹, Theresa R. Connors², Derek H. Oakley², Bradley T. Hyman², Oula Puonti^{1,5}, Matthew S. Rosen¹, and Juan Eugenio Iglesias^{1,3,4}

¹ Martinos Center for Biomedical Imaging, Massachusetts General Hospital and Harvard Medical School

² Massachusetts Alzheimer’s Disease Research Center, Massachusetts General Hospital and Harvard Medical School

³ Hawkes Institute, University College London

⁴ Computer Science and Artificial Intelligence Laboratory, Massachusetts Institute of Technology

⁵ Danish Research Centre for Magnetic Resonance, Centre for Functional and Diagnostic Imaging and Research, Copenhagen University Hospital—Amager and Hvidovre, Copenhagen, Denmark

Abstract. Correlation of neuropathology with MRI has the potential to transfer microscopic signatures of pathology to *in vivo* scans. Recently, a classical registration method has been proposed, to build these correlations from 3D reconstructed stacks of dissection photographs, which are routinely taken at brain banks. These photographs bypass the need for *ex vivo* MRI, which is not widely accessible. However, this method requires a full stack of brain slabs and a reference mask (e.g., acquired with a surface scanner), which severely limits the applicability of the technique. Here we propose “RefFree”, a dissection photograph reconstruction method without external reference. RefFree is a learning approach that estimates the 3D coordinates in the atlas space for every pixel in every photograph; simple least-squares fitting can then be used to compute the 3D reconstruction. As a by-product, RefFree also produces an atlas-based segmentation of the reconstructed stack. RefFree is trained on synthetic photographs generated from digitally sliced 3D MRI data, with randomized appearance for enhanced generalization ability. Experiments on simulated and real data show that RefFree achieves performance comparable to the baseline method without an explicit reference while also enabling reconstruction of partial stacks. Our code is available at <https://github.com/lintian-a/refree>.

Keywords: Neuroimaging-pathology correlation · Joint registration.

1 Introduction

Neuropathology (microscopic examination of brain tissue *post mortem*) is the gold standard diagnosis of neurodegenerative diseases. There are two phases in

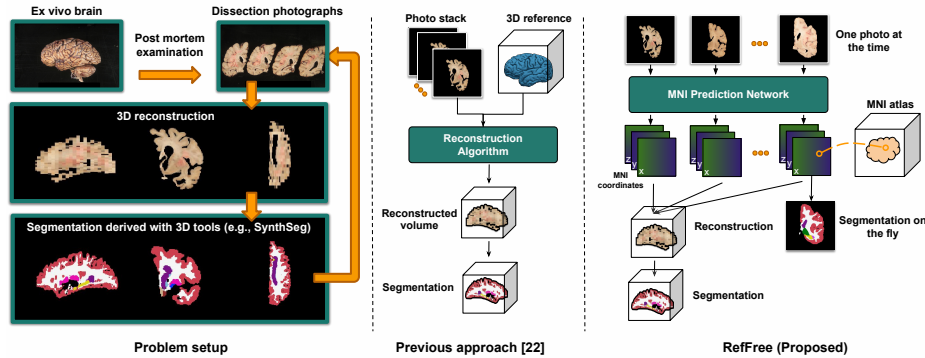


Fig. 1: Problem setup and approach. In our problem (left), we are given a stack of dissection photographs, which we aim to reconstruct into a 3D brain volume with its structures labeled. Previous methods (middle) require a reference image (e.g., a surface or permortem MRI scan) to guide this 3D reconstruction. The proposed method (right) solves this problem using a neural network that receives only the photographs as input and outputs predictions of voxel coordinates in MNI space, which are fit to a transform for 3D reconstruction.

postmortem examination: (a) gross examination of dissected brain slabs (typically coronal, with thicknesses between 5 and 10 mm, see Fig. 1), and (b) microscopic histological examination of selected sections, cut from tissue blocked from the slabs. Estimating a spatial correspondence between microscopic images and macroscopic 3D images of the brain (e.g., MRI) has important applications neuropathology-neuroimaging correlation studies, which seek to bring microscopic signatures of pathology to *in vivo* scans to discover novel imaging biomarkers [5,17]. These studies currently require an MRI scan, acquired either *post mortem* (cadaveric [21] or *ex vivo* [7]) or *peri mortem* (i.e., *in vivo* soon before death). However, none of these modalities is widely accessible [22,11].

A cost-effective and accessible modality is dissection photography, which is acquired routinely at brain banks. These are 2D photographs of the slab surfaces taken during dissection. It has been recently shown that these photographs can be used to reconstruct an imaging volume, i.e., a *pseudo-MRI* that enables 3D image analysis [22,11]. This method is publicly available on FreeSurfer [8] and relies on iterative optimization of an objective function that combines a slab-to-slab similarity with a reference mask – acquired with a 3D surface scanner or, alternatively, a generic probabilistic atlas. However, this approach has two main limitations. First, it requires the availability of the complete stack of photographs, which precludes application to incomplete sets of images – or, in an extreme case, single slab photographs. And second, the segmentation maps can only be extracted after solving the reconstruction.

Here we present RefFree, a learning-based method that tackles the above limitations. Given a photograph and its approximate anterior-posterior (y) co-

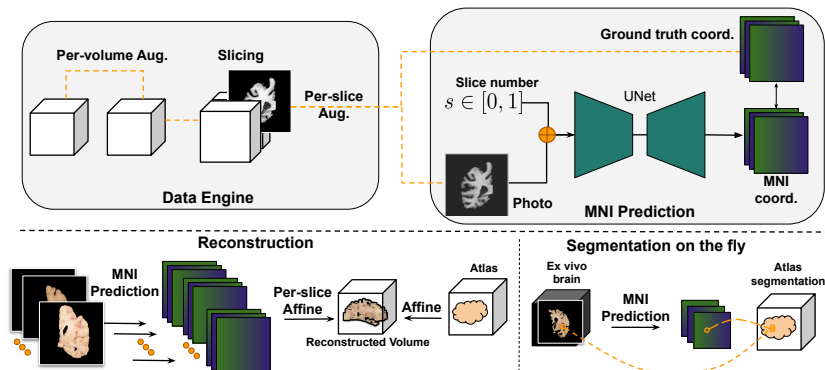


Fig. 2: Training and inference. During training (top), synthetic photographs are generated by digitally slicing brain MRI scans at planes with random but known MNI coordinates. A U-Net is trained with the generated photographs as input and the plane of MNI coordinates as targets. At inference (bottom), the U-Net receives a stack (batch) of dissection photographs to predict a stack of MNI voxel coordinates from which the 3D reconstruction can be analytically computed.

ordinate on the stack (estimated, e.g., by the slab number), a convolutional neural network (CNN) estimates the 3D coordinates in atlas space (MNI) for every pixel. Given these predicted coordinates, efficient least squares updates can be used to analytically compute the reconstruction of a full or partial stack of photographs. Compared with the FreeSurfer method, RefFree handles partial stacks and yields an atlas-based segmentation as a by-product. Moreover, our synthetic data engine mitigates the data scarcity in human dissection photography and paves the way for new learning-based tools for image analysis in this domain.

2 Method

Reffree comprises two modules (Fig. 2). The first one is a CNN that estimates the 3D atlas (MNI) coordinates of each pixel in a 2D slab photograph (Sec. 2.1). Crucially, photographs are analyzed by CNN independently, which enables processing of partial stacks or even single images. Given these predictions for a set of photographs of a specimen, the second module analytically fits a set of transformations that jointly bring the 2D photographs into 3D MNI space (Sec. 2.2).

2.1 MNI Coordinate Prediction of Dissection Photographs

Task formulation. Let $I : \Omega_s \rightarrow R$, $\Omega_s : [-1, 1]^2$ be a grayscale 2D image, and let $s \in [0, 1]$ be its normalized slice number from posterior to anterior. This slice number serves as a coarse coordinate to condition the prediction. Its normalization enables the analysis of specimens with different numbers of

photographs due to differences in brain size or slab thickness. Given a dataset of I, s pairs, we train a CNN to predict the corresponding coordinate of each pixel in Ω_s within the 3D atlas space $\Omega_t : [-1, 1]^3$, i.e., $f_\theta(I, s) = Y, Y : \Omega_s \rightarrow \Omega_t$.

Synthetic Data Engine for Training. Preparing a real dataset with sufficiently diverse slab photographs (different cameras, illumination conditions, cutting angles...) would be extremely impractical – and so would be to obtain ground truth MNI coordinates. Instead, we use a synthetic dataset built from MRI. High-resolution T1-weighted scans are widely available and enable: *(i)* Accurate estimation of ground truth MNI coordinates via classical nonlinear registration; *(ii)* Accurate automated segmentation for subsequent simulation of synthetic photographs (details below); and *(iii)* Simulation of a virtually infinite pool of cutting angles and slab thicknesses during training. Given a set of label maps, domain randomization has been shown to be a highly effective approach to train CNNs for generalizable image analysis [2,14,19]. The core idea is to generate synthetic MRI with random contrast by sampling a Gaussian Mixture Model (GMM) conditioned on digitally slabbed segmentations.

Specifically: *(i)* MNI coordinates and 3D segmentation maps are estimated with FreeSurfer [8], and the MNI maps are masked with the segmentation; *(ii)* we augment the 3D segmentations with labels of the claustrum (obtained with multi-atlas segmentation [15]) and limbic structures (obtained with a neural network [13]); *(iii)* during training, we augment the 3D segmentations and MNI maps with random 3D affine transformations (we note that the rigid component of the transform models the cutting angle); *(iv)* we digitally slab the label map (and corresponding ground truth MNI maps) and add further slab-wise deformations; and *(v)* we synthesize photographs with the GMM, combined with a smooth multiplicative field that simulates uneven lighting conditions, followed by *(vi)* random cropping. At every minibatch, the network sees tuples $\{(I_i, s_i, Y_i)\}$ with a 2D image, a slice number, and an MNI map.

CNN Training. We minimize the mean absolute error between the predicted and ground truth MNI coordinates, averaged over foreground pixels:

$$\mathcal{L} = \sum_{i=0}^N \frac{1}{\|M_i\|_1} \|M_i \odot (f_\theta(I_i, s_i) - Y_i)\|_1, \quad (1)$$

where M_i is the foreground mask. We train for 100 epochs with Adam ($\eta = 10^{-4}$).

Inference on Real Photographs. Real photographs are first preprocessed by converting to grayscale, min-max normalization, correcting for pixel size and perspective, segmenting the foreground, and ordering from anterior to posterior, all achieved with FreeSurfer tools [1]. The normalized, masked images and slice numbers are input into the CNN to predict the MNI maps.

2.2 3D Reconstruction

Given the predicted MNI coordinates for a set of slabs, 3D reconstruction can be formulated as a joint fitting problem: what set of 3D affine transforms $\{A_i^{3D}\}$ yield a 3D reconstruction, where pixels are as close as possible to their predicted MNI coordinates in the least squares sense? A crucial aspect of this problem is the prior knowledge that the slabs are approximately parallel. Rather than optimizing for $\{A_i^{3D}\}$ directly under this constraint, we instead rewrite A_i^{3D} as a product of a 2D slab-specific transform A_i^{2D} in plane, and a global 3D affine transform A that is common to all slabs, i.e., $A_i^{3D} = AA_i^{2D}$. This guarantees that the slabs are parallel in the 3D reconstruction, and enables a simple coordinate descent scheme where every update is computed in closed form using least squares regression (A given $\{A_i^{2D}\}$, and A_i^{2D} given A – one i at the time).

3 Experiments

We evaluate RefFree qualitatively and quantitatively on real and simulated data:

Brain MRI Composite Dataset. For training, we curated a dataset from 11 brain MRI repositories (ABIDE [6], ADHD200 [3], ADNI [16,25], AIBL [10], FreeSurfer [9], COBRE [20], Chinese-HCP [24], HCP [23], ISBI2015 [4], MCIC [12], OASIS3 [18]), all of which include 1 mm isotropic T1w scans. These were pre-processed with FreeSurfer [8] as explained in Section 2.1 to obtain the training data. After manual quality control of the FreeSurfer outputs, we included 5,279 total subjects. We made a training/validation/test split with 4,217/862/200 scans.

Simulated Dissection Photographs. We simulate *ex vivo* photographs for evaluation using the Brain MRI composite dataset (validation and test sets) following the procedure in [11] (Fig. 4). Using slightly different approaches to generate the *simulated* photographs for evaluation and *synthetic* images for training enables us to mimic the domain gap between training and inference in real scenarios.

Real Dissection Photographs. We took photographs of coronal slabs of 8 cases from NEUROPATHOLOGY-LAB-X. These are thick (~ 10 mm) slabs, which makes 3D reconstruction challenging.

3.1 Evaluation with Simulated Brain Dissection Photographs

We evaluate two separate aspects of RefFree: the ability of the U-net to predict MNI coordinates, and the accuracy of the full pipeline in 3D reconstruction.

MNI Coordinate Prediction. We compute the mean squared error (MSE) between the predicted and ground truth coordinates, and the Dice score between label maps warped by the predicted and ground truth segmentations (Fig. 3). The overall mean MSE on the test set across datasets is ~ 22 , i.e., root MSE

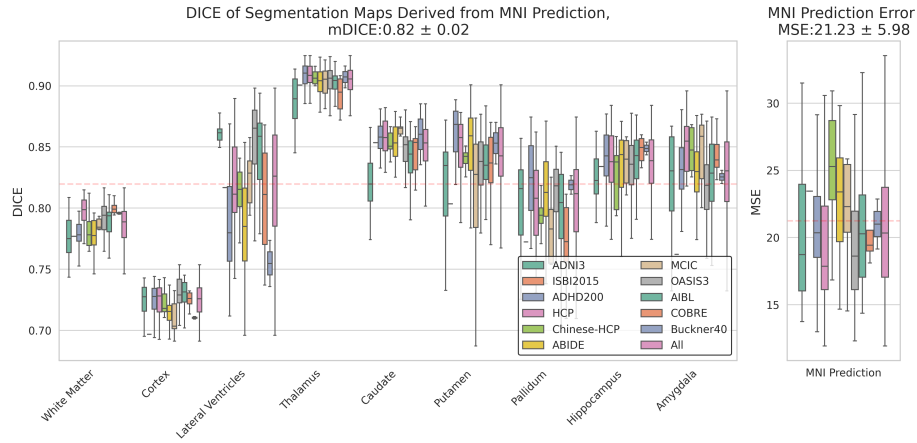


Fig. 3: Prediction error quantified using MSE and Dice. The MSE plots (right) show that the MNI coordinates predicted by RefFree are accurate to within X mm on average. Dice scores of select structures (left) show that the resulting brain reconstructions correlate strongly with the underlying brain volumes.

under 5 mm, which is quite accurate, considering the difficulties of estimating the y coordinates out of plane. The average Dice is .82, averaged over 9 representative structures of interest. The figure shows that the U-net performs consistently well across highly heterogeneous populations, including healthy subjects (HCP, Chinese-HCP), dementia (OASIS3, ADNI3, AIBL, FreeSurfer), Autism Spectrum Disorder (ABIDE), Attention Deficit Hyperactivity Disorder (ADHD), Schizophrenia (COBRE, MCIC), and Multiple Sclerosis (ISBI2015).

3D Reconstruction. We adopt two references to evaluate the reconstruction with the MNI prediction algorithm (Sec. 2.2) on the test set: (1) a silver standard consisting of the volume reconstructed from the ground truth MNI coordinates, and (2) a gold standard consisting of the MRI used to simulate the photographs. We compute the MSE and Structural similarity index measure (SSIM) between the RefFree reconstruction and both references (Tab. 1, with visual results shown in Fig. 4). The reconstructed volume closely matches the silver standard (SSIM: 0.85 for the test dataset), while the SSIM with the gold standard is lower but similar to that between the silver and gold references (a proxy for the upper bound of the performance). Part of the remaining gap is likely due to only modeling affine transformations (as shown in Fig. 2).

Ablation Study of The Data Engine. We perform an ablation study on the augmentations used in the synthetic data engine, measuring the MNI coordinate prediction error (Tab. 2). All augmentations increase performance, but cropping and intensity augmentation are the largest contributors.

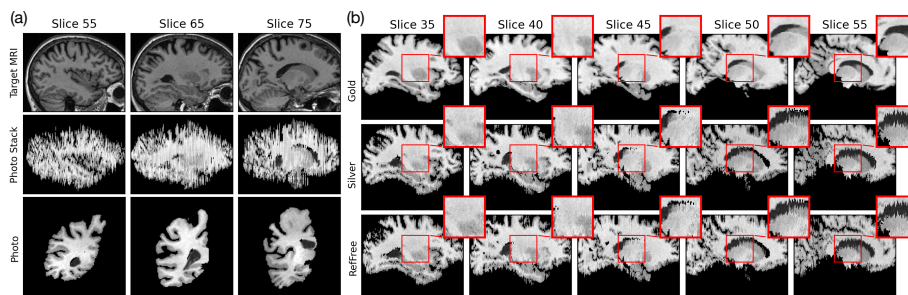


Fig. 4: Visualization of RefFree reconstruction: (a) simulated photograph stack (coronal view) and photographs; (b) RefFree reconstruction (coronal view) compared to silver and gold standard references given the case shown in (a).

Table 1: RefFree reconstruction evaluation on the simulated test dataset. The silver standard refers to the volume reconstructed by RefFree using the ground truth MNI coordinates, while the gold standard represents the MRI volume used to generate the simulated photographs.

	Silver		Gold	
	MSE↓	SSIM↑	MSE↓	SSIM↑
Initial	5.16e-1	0.12	1.31e-1	0.52
Silver			2.14e-2	0.77
RefFree	1.10e-2	0.85	2.04e-2	0.78

Table 2: The ablation study of the augmentation used during training. I: Intensity augmentation. D: Deformation augmentation. A: Affine augmentation. C: Central crop. R: Random crop.

Ablation Study	MSE↓
Baseline	4126.52
+I	1126.67
+I/D	1127.76
+I/D/A	1082.72
+I/D/A/C	25.28
+I/D/A/R	24.71

3.2 Applications with Real *ex vivo* Brain Dissection Photographs

In this section, we demonstrate RefFree on 3 applications using the real dataset. We compare our method with the optimization-based method in FreeSurfer, using the same MNI atlas as 3D reference.

3D Reconstruction of Slab Photographs. Reconstructing a 3D volume from slab photographs is a crucial first step in taking advantage of established brain image analysis tools designed for 3D images. In this experiment, we reconstruct a volume from a full stack of photographs and estimate its segmentation using SynthSeg. We compare the volume sizes derived from RefFree’s reconstruction with those from a reference-based baseline [22,11] as shown in Tab. 3 and visualize one case in Fig. 5-a. The results demonstrate a high correlation between RefFree and the baseline, indicating that RefFree is a viable alternative when reference data are unavailable.

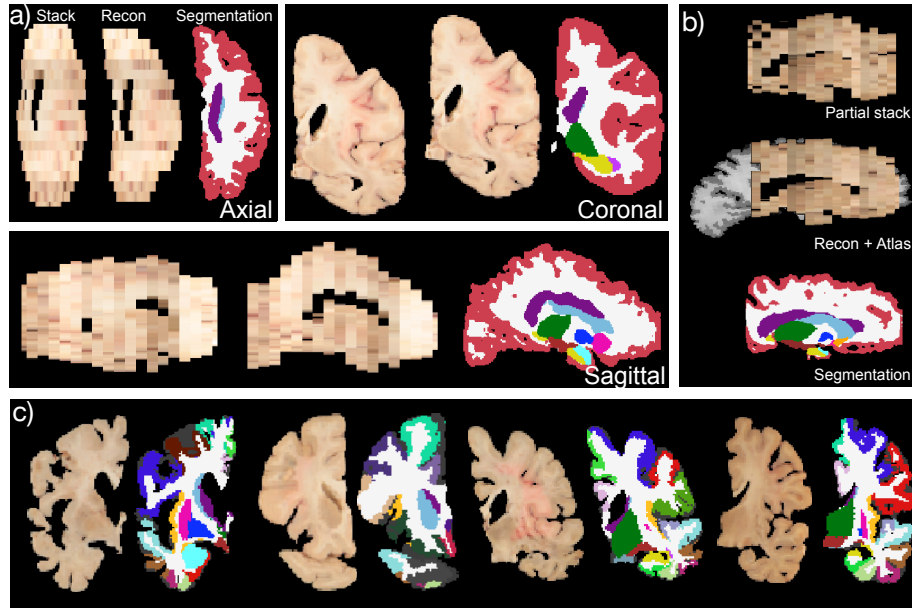


Fig. 5: Qualitative results of RefFree on 6 real cases in (a) reconstruction from a full stack of photographs, (b) reconstruction from a partial stack, and (c) segmentation of single photograph on the fly (without reconstruction).

3D Reconstruction with a Partial Brain Slab Stack. RefFree can also handle incomplete brain slab stacks – a common scenario in archived photographic data, which the FreeSurfer method cannot handle. RefFree’s capability by reconstructing a volume from a partial stack is shown in Fig. 5-(b).

Realtime Segmentation Computation during Brain Slab Cutting. During brain cutting, real-time segmentation maps projected onto the slab could assist pathologists in locating anatomical structures for tissue sampling (digitally-guided dissection), particularly in cortical regions. This is not possible with the existing FreeSurfer method. Using RefFree, we demonstrate this capability by computing a warped atlas segmentation using the predicted MNI coordinates (Fig. 5-c).

Table 3: Pearson correlation of the volumes of brain structures, derived from the SynthSeg segmentations of the 3D reconstructions obtained with the optimization-based method in FreeSurfer [22] (baseline) and RefFree.

	Wh.Ma.	Cortex	Lat.	Vent.	Thal.	Caud.	Put.	Pallid.	Hippo.	Amyg.
RefFree	0.989	0.997	0.992	0.970	0.893	0.942	0.905	0.991	0.966	

4 Conclusion

We propose RefFree, a reference-free 3D reconstruction method for dissection photographs trained on *purely synthetic data*. RefFree serves as a viable alternative to the existing reference-based method in FreeSurfer for full-stack reconstruction, while also addressing scenarios where the baseline method falls short (e.g., partial stacks), offering a versatile tool for postmortem brain examination. RefFree also has limitations, such as its reliance on slice indices and its current inability to account for non-rigid deformations during reconstruction. Future work will explore: eliminating the dependency on slice indices; modeling nonlinear deformation, which is crucial when cutting fresh rather than fixed tissue; better simulation of dissection photography using 3D models of slices and photorealistic rendering; and further validation on downstream applications. In conclusion, this study lays the foundation for robust and generalizable reference-free reconstruction from brain dissection photographs using machine learning.

4.1 Acknowledgments.

This work was supported by NIH under grant 1RF1MH123195, 1R01AG070988, 1R01EB031114, 1UM1MH130981, 1RF1AG080371, 1R21NS138995, and MADRC grant P30 AG062421. Sean I. Young is supported by NIH K99AG081493. Matthew S. Rosen acknowledges the generous support of the Kiyomi and Ed Baird MGH Research Scholar award. Oula Puonti is supported by a grant from the Lundbeck Foundation (R360-2021-39). The content of this publication is solely the responsibility of the authors and does not necessarily represent the official views of the funding agency.

References

1. Photo reconstruction documentation. <https://surfer.nmr.mgh.harvard.edu/fswiki/PhotoTools>, accessed: 2025-02-20
2. Billot, B., Greve, D.N., Puonti, O., Thielscher, A., Van Leemput, K., Fischl, B., Dalca, A.V., Iglesias, J.E., et al.: Synthseg: Segmentation of brain mri scans of any contrast and resolution without retraining. *Medical image analysis* **86**, 102789 (2023)
3. Brown, M.R., Sidhu, G.S., Greiner, R., Asgarian, N., Bastani, M., Silverstone, P.H., Greenshaw, A.J., Dursun, S.M.: Adhd-200 global competition: diagnosing adhd using personal characteristic data can outperform resting state fmri measurements. *Frontiers in systems neuroscience* **6**, 69 (2012)
4. Carass, A., Roy, S., Jog, A., Cuzzocreo, J.L., Magrath, E., Gherman, A., Button, J., Nguyen, J., Prados, F., Sudre, C.H., et al.: Longitudinal multiple sclerosis lesion segmentation: resource and challenge. *NeuroImage* **148**, 77–102 (2017)
5. Dawe, R.J., Bennett, D.A., Schneider, J.A., Arfanakis, K.: Neuropathologic correlates of hippocampal atrophy in the elderly: a clinical, pathologic, postmortem mri study. *PloS one* **6**(10), e26286 (2011)
6. Di Martino, A., Yan, C.G., Li, Q., Denio, E., Castellanos, F.X., Alaerts, K., Anderson, J.S., Assaf, M., Bookheimer, S.Y., Dapretto, M., et al.: The autism brain imaging data exchange: towards a large-scale evaluation of the intrinsic brain architecture in autism. *Molecular psychiatry* **19**(6), 659–667 (2014)
7. Edlow, B.L., Mareyam, A., Horn, A., Polimeni, J.R., Witzel, T., Tisdall, M.D., Augustinack, J.C., Stockmann, J.P., Diamond, B.R., Stevens, A., et al.: 7 tesla mri of the ex vivo human brain at 100 micron resolution. *Scientific data* **6**(1), 244 (2019)
8. Fischl, B.: FreeSurfer. *Neuroimage* **62**(2), 774–781 (2012)
9. Fischl, B., Salat, D.H., Busa, E., Albert, M., Dieterich, M., Haselgrove, C., Van Der Kouwe, A., Killiany, R., Kennedy, D., Klaveness, S., et al.: Whole brain segmentation: automated labeling of neuroanatomical structures in the human brain. *Neuron* **33**(3), 341–355 (2002)
10. Fowler, C., Rainey-Smith, S.R., Bird, S., Bomke, J., Bourgeat, P., Brown, B.M., Burnham, S.C., Bush, A.I., Chadunow, C., Collins, S., et al.: Fifteen years of the australian imaging, biomarkers and lifestyle (aibl) study: progress and observations from 2,359 older adults spanning the spectrum from cognitive normality to alzheimer’s disease. *Journal of Alzheimer’s disease reports* **5**(1), 443–468 (2021)
11. Gazula, H., Tregidgo, H.F., Billot, B., Balbastre, Y., Williams-Ramirez, J., Herisse, R., Deden-Binder, L.J., Casamitjana, A., Melief, E.J., Latimer, C.S., et al.: Machine learning of dissection photographs and surface scanning for quantitative 3d neuropathology. *eLife* **12**, RP91398 (2024)
12. Gollub, R.L., Shoemaker, J.M., King, M.D., White, T., Ehrlich, S., Sponheim, S.R., Clark, V.P., Turner, J.A., Mueller, B.A., Magnotta, V., et al.: The mcic collection: a shared repository of multi-modal, multi-site brain image data from a clinical investigation of schizophrenia. *Neuroinformatics* **11**, 367–388 (2013)
13. Greve, D.N., Billot, B., Cordero, D., Hoopes, A., Hoffmann, M., Dalca, A.V., Fischl, B., Iglesias, J.E., Augustinack, J.C.: A deep learning toolbox for automatic segmentation of subcortical limbic structures from mri images. *Neuroimage* **244**, 118610 (2021)
14. Iglesias, J.E., Billot, B., Balbastre, Y., Magdamo, C., Arnold, S.E., Das, S., Edlow, B.L., Alexander, D.C., Golland, P., Fischl, B.: Synthsr: A public ai tool to turn

- heterogeneous clinical brain scans into high-resolution t1-weighted images for 3d morphometry. *Science advances* **9**(5), eadd3607 (2023)
15. Iglesias, J.E., Sabuncu, M.R.: Multi-atlas segmentation of biomedical images: a survey. *Medical image analysis* **24**(1), 205–219 (2015)
 16. Jack Jr, C.R., Bernstein, M.A., Fox, N.C., Thompson, P., Alexander, G., Harvey, D., Borowski, B., Britson, P.J., L. Whitwell, J., Ward, C., et al.: The alzheimer’s disease neuroimaging initiative (adni): Mri methods. *Journal of Magnetic Resonance Imaging: An Official Journal of the International Society for Magnetic Resonance in Medicine* **27**(4), 685–691 (2008)
 17. Kotrotsou, A., Schneider, J.A., Bennett, D.A., Leurgans, S.E., Dawe, R.J., Boyle, P.A., Golak, T., Arfanakis, K.: Neuropathologic correlates of regional brain volumes in a community cohort of older adults. *Neurobiology of aging* **36**(10), 2798–2805 (2015)
 18. LaMontagne, P.J., Benzinger, T.L., Morris, J.C., Keefe, S., Hornbeck, R., Xiong, C., Grant, E., Hassenstab, J., Moulder, K., Vlassenko, A.G., et al.: Oasis-3: longitudinal neuroimaging, clinical, and cognitive dataset for normal aging and alzheimer disease. medrxiv pp. 2019–12 (2019)
 19. Liu, P., Puonti, O., Hu, X., Alexander, D.C., Iglesias, J.E.: Brain-id: Learning contrast-agnostic anatomical representations for brain imaging. In: *European Conference on Computer Vision*. pp. 322–340. Springer (2024)
 20. Mayer, A.R., Ruhl, D., Merideth, F., Ling, J., Hanlon, F.M., Bustillo, J., Canive, J.: Functional imaging of the hemodynamic sensory gating response in schizophrenia. *Human brain mapping* **34**(9), 2302–2312 (2013)
 21. Ruder, T.D., Thali, M.J., Hatch, G.M.: Essentials of forensic post-mortem mr imaging in adults. *The British journal of radiology* **87**(1036), 20130567 (2014)
 22. Tregidgo, H.F., Casamitjana, A., Latimer, C.S., Kilgore, M.D., Robinson, E., Blackburn, E., Van Leemput, K., Fischl, B., Dalca, A.V., Donald, C.L.M., et al.: 3d reconstruction and segmentation of dissection photographs for mri-free neuropathology. In: *Medical Image Computing and Computer Assisted Intervention—MICCAI 2020: 23rd International Conference, Lima, Peru, October 4–8, 2020, Proceedings, Part V* 23. pp. 204–214. Springer (2020)
 23. Van Essen, D.C., Ugurbil, K., Auerbach, E., Barch, D., Behrens, T.E., Bucholz, R., Chang, A., Chen, L., Corbetta, M., Curtiss, S.W., et al.: The human connectome project: a data acquisition perspective. *Neuroimage* **62**(4), 2222–2231 (2012)
 24. Vogt, N.: The chinese human connectome project. *Nature Methods* **20**(2), 177–177 (2023)
 25. Weiner, M.W., Veitch, D.P., Aisen, P.S., Beckett, L.A., Cairns, N.J., Green, R.C., Harvey, D., Jack Jr, C.R., Jagust, W., Morris, J.C., et al.: The alzheimer’s disease neuroimaging initiative 3: Continued innovation for clinical trial improvement. *Alzheimer’s & Dementia* **13**(5), 561–571 (2017)